Isothermal Fatigue Behavior of a [90]8 SiC/Ti–15–3 Composite at 426 °C

John Gayda and Timothy P. Gabb
Lewis Research Center
Cleveland, Ohio

January 1991

NASA

ISOTHERMAL FATIGUE BEHAVIOR OF A $[90]_8$ SiC/Ti-15-3 COMPOSITE AT 426 °C

John Gayda and Timothy P. Gabb
National Aeronautics and Space Administration
Lewis Research Center
Cleveland, Ohio 44135

SUMMARY

The transverse fatigue behavior of a unidirectional, SiC/Ti-15-3 composite (35 vol % SiC, $[90]_8$) was evaluated at 426 °C. The fatigue behavior of the composite along the fiber direction ($[0]_8$) and of unreinforced Ti-15-3 alloy were also studied for comparison purposes. The $[90]_8$ composite fatigue life was much shorter than $[0]_8$ life. Further, $[90]_8$ fatigue life was also found to be far lower than that of the unreinforced Ti-15-3 alloy. A simple, one-dimensional model for $[90]_8$ fatigue behavior indicated that the short life of the composite in this orientation resulted, in large part, from weak fiber-matrix bond strength. This conclusion was supported by fractographic evidence showing numerous fatigue initiation sites along the fiber-matrix interfaces.

INTRODUCTION

Composites of titanium matrix reinforced with SiC fibers have recently received considerable attention as candidate materials in advanced aerospace applications (ref. 1). One such application involves compressor disks, where elevated temperature fatigue considerations are important. While the fatigue properties of unidirectional SiC/Ti matrix composites loaded parallel to the fibers are promising (refs. 2 to 4), the fatigue properties in loading transverse to the fibers are a possible problem (ref. 4) and have received much less attention, experimentally and analytically. Low fiber-matrix bond strength in SiC/Ti matrix composites has been cited as a contributory factor leading to low transverse fatigue strength. At elevated temperatures, creep and plasticity of the matrix may also affect transverse fatigue strength.

The purpose of the present study is to characterize and understand the transverse fatigue behavior of a unidirectional SiC/Ti-15-3 composite at 426 °C. Fatigue life data for the unreinforced Ti-15-3 alloy and the composite along the fiber direction will also be assessed for comparative purposes. These comparisons will be made on a stress and strain basis where appropriate. To augment understanding of fatigue behavior in the transverse direction, a simple one-dimensional model was developed and employed to separate the roles of fiber-matrix debonding, matrix flow, and matrix creep.

MATERIALS AND PROCEDURES

The composite used in this study had a Ti-15V-3Cr-3Al-3Sn alloy matrix (by weight percent), reinforced by 35 vol % of continuous SiC fiber, SCS-6. A detailed description of the composite microstructure is contained elsewhere (ref. 5). All composite test specimens used in this study were obtained from a single eight-ply, unidirectional panel manufactured by Textron Specialty Materials Division using a fiber-foil approach in which fiber alignment was

maintained with the use of a fugitive binder. Textron also fabricated an unreinforced Ti-15-3 alloy plate, using Ti-15-3 foil and the same consolidation parameters employed in composite production.

Flat composite test specimens shown in figure 1 were machined from the composite panel using a two-step process. A slightly oversized specimen was cut out using a wire EDM procedure and then diamond ground to remove damaged material. Specimens were machined with the fibers parallel ($[0]_8$) and perpendicular ($[90]_8$) to the 153-mm loading axis dimension. For testing unreinforced Ti-15-3 alloy, the cylindrical specimen geometry shown in figure 2 was employed. All specimens were subsequently heat treated at 700 °C for 24 hr in vacuum.

Tensile and fatigue tests of composite specimens were run at 426 °C using a closed-loop, servohydraulic test system equipped with hydraulic wedge grips. Strain or load was employed as the closed-loop test control variable. Direct induction heating was used and specimen temperature was controlled with an infrared pyrometer. Axial strain measurements were made with a high temperature extensometer having a 12.5-mm gage length. The Ti-15-3 alloy specimens were also tested using a closed-loop, servohydraulic test system. However, a furnace/hot grip system was employed in these tests. For both composite and Ti-15-3 alloy tests, stress versus strain hysteresis loops were periodically recorded using an x-y recorder. In addition, stress versus time and strain versus time data were continually recorded with a two-pen strip chart recorder.

RESULTS

Monotonic Testing

Tensile tests on the composite and Ti-15-3 alloy were run at a constant strain rate of 0.1 percent per second. The tensile stress-strain curves for the $[90]_8$ composite and the Ti-15-3 alloy are presented in figure 3. Note the initial modulus of the composite is significantly greater than that of the Ti-15-3 alloy, however, the composite response becomes nonlinear at a lower stress. Further, the $[90]_8$ composite also has a much lower fracture strength and strain than the Ti-15-3 alloy. Tensile testing was also done on $[0]_8$ composite for comparative purposes. The fracture strength and strain in this orientation was 1510 MPa and 0.87 percent, respectively. Compared to the $[90]_8$ composite or the Ti-15-3 alloy, the stress-strain response of the $[0]_8$ composite was essentially linear.

Stress relaxation tests were also run on the Ti-15-3 alloy at 426 °C to estimate time-dependent properties of the Ti-15-3 matrix in the composite. In these tests a Ti-15-3 alloy specimen was loaded to 172, 344, or 517 MPa at a rate of 0.1 percent per second and then held at the resulting strain level for extended periods of time. The subsequent stress-time response of the Ti-15-3 alloy is presented in figure 4. The stress relaxation data for all three initial stress levels can be approximated by a single curve after shifting the time scales at 172 and 344 MPa.

2

Load-Controlled Fatigue Testing

Zero-tension, load-controlled fatigue tests were run on composite specimens using a sawtooth control waveform having a frequency of 0.3 Hz. These tests were run on $[90]_8$ composite as well as $[0]_8$ composite for comparative purposes. For both orientations, fatigue life was defined to be the number of cycles required to completely fracture the specimen. Fatigue life versus stress range data are presented in figure 5. Note that fatigue life for the $[90]_8$ orientation is significantly less than that for the $[0]_8$ orientation.

The cyclic stress-strain response of a typical $[90]_8$ composite test at a stress range of 138 MPa is presented in figure 6. As this test lasted 3603 cycles, the stress-strain loops at 1500 and 3500 cycles depict composite behavior near half-life and failure, respectively. A significant amount of irreversible strain was produced during cycle one. In subsequent cycles, the irreversible strain generated in each cycle was below the detectable level, even though stress-strain behavior was measurable nonlinear. However, as seen in figure 7, a sizeable change in both the minimum and maximum strain is produced over the life of the test. This change reflects a decrease in composite stiffness and a gradual increase in mean strain. Similar behavior was also observed in tests at other stress ranges as shown in figure 8. The cyclic stress-strain response of $[0]_8$ composite at elevated temperatures is thoroughly discussed in reference 6.

Strain-Controlled Fatigue Testing.

Zero-tension, strain-controlled fatigue tests of $[90]_8$ composite specimens were also run using a sawtooth control waveform having a frequency of 0.3 Hz. Unlike the load-controlled tests, fatigue life of strain-controlled $[90]_8$ composite tests was defined as the number of cycles required to produce a 75-percent reduction in peak stress. Such a definition was required because the peak stress would gradually approach zero without producing complete specimen fracture. A 75-percent reduction criteria was used as relaxation could produce a 50-percent reduction in peak stress without significant levels of fatigue cracking/damage. Strain-controlled fatigue tests were also run on Ti-15-3 alloy specimens for comparison purposes. Fatigue life is presented as a function of strain range in figure 9. In addition to the strain-controlled test data, the load-controlled fatigue life data for the $[90]_8$ composite and the $[0]_8$ composite are also plotted using the measured strain range at half-life. With the exception of the strain-controlled $[90]_8$ composite life line, all other fatigue lives were defined by complete specimen fracture. From this strain-based life comparison, it is obvious that the fatigue life of the $[90]_8$ composite is far lower than that of the $[0]_8$ composite or the Ti-15-3 alloy irrespective of control mode.

The cyclic stress-strain response of a typical strain-controlled $[90]_8$ composite test at a strain range of 0.28 percent is presented in figure 10. The stress-strain loop at 3000 cycles is near half-life while that at 6000 cycles is very near the defined fatigue life of 6300 cycles. As stated previously, the fatigue life represents the point at which the peak stress has dropped by 75 percent rather than specimen fracture. A significant amount of irreversible strain is generated in cycle one. In subsequent cycles, very little hysteresis is observed. However, a gradual decrease in mean stress and

tensile stiffness is observed over the duration of the test. Note that the compressive stiffness is much greater than the tensile stiffness later in the test. The decreases in mean stress and tensile stiffness are reflected in the changing stress levels shown in figure 11. The composite could be cycled well beyond the defined fatigue life of 6300 cycles, although the maximum stress becomes very low. By $N = 10\ 000$ the peak stress was less than 10 MPa and a large crack was readily observable. The stress-strain response of other $[90]_8$ composite specimens tested under strain control was similar as shown in figure 12.

ANALYSIS AND DISCUSSION

An examination of monotonic and cyclic deformation behavior of the $[90]_8$ composite suggests that fiber-matrix interface failure initiates the nonlinear response. This hypothesis is supported by two observations. First, the initial nonlinearity in the stress-strain curve of the $[90]_8$ composite occurs at a significantly lower strain than that of the Ti-15-3 alloy shown in figure 3. Second, the unloading modulus on cycle one is significantly less than the initial modulus as shown in figure 10. With continued cycling it was noted that the mean stress decreased in strain-controlled tests, while mean strain increased in stress-controlled tests. This behavior could be produced by matrix creep and/or crack growth.

From the above discussion it is clear that a model for $[90]_8$ composite behavior which includes matrix flow, matrix creep, and fiber-matrix debonding would be helpful in understanding mechanical response. Numerous finite element analysis (refs. 7 and 8) of transverse composite behavior have been run using a unit cell containing one to several fibers. Some of these analyses have included matrix flow and/or fiber-matrix debonding and have successfully simulated tensile behavior of $[90]_n$ composite behavior. However, this type of analysis would be impractical for analyzing fatigue data over thousands of cycles, especially when time-dependent phenomenon is included. To overcome this problem, a simple one-dimensional analysis of $[90]_8$ composite behavior will be used.

Model Concepts

A simple one-dimensional model for $[90]_n$ composite behavior can be easily formulated to include plasticity, debonding, and creep effects, as well as effects associated with irregular fiber distribution. The basic approach of this type of analysis is schematically represented in figure 13. Alternate rows of matrix elements and fiber-matrix elements are used to simulate the composite. Individual fiber-matrix elements have variable fiber contents, L_f, to simulate stress concentration effects in the matrix associated with experimentally observed variations in fiber spacing and hence local fiber content. The overall fiber content of the model is held at 0.35.

To use the composite model, an increment of external load is first applied along the x-direction as shown in figure 13. The columns are loaded in series in this model. Therefore, the load transmitted normal to all columns must be the same and equal to the external load. Overall compatibility is maintained by requiring the displacements of all elements within a column to be identical.

4

Therefore, the elements of each column are loaded in parallel. The displacement of each column is then obtained by dividing the load increment by the total column stiffness. The composite displacement is, in turn, calculated by summing the displacements of all columns in the series model.

The column stiffness is obviously very important in this model and is calculated by summing the individual elements stiffnesses within a given column. The stiffness of a fiber-matrix element K_e is defined as follows:

$$K_e = \frac{1}{\left(\dfrac{L_f}{E_f} + \dfrac{(1 - L_f)}{E_m} \right)}$$

where E_f is the fiber modulus and E_m is the matrix modulus for an element of unit length and width. The fiber content, L_f, is equal to 0 for a matrix element. Matrix plasticity is simulated by setting E_m equal to a plastic modulus when an element stress exceeds the yield strength of the Ti-15-3 alloy; otherwise E_m is equal to the elastic modulus of the Ti-15-3 alloy. A simple, isotropic hardening rule governing matrix flow was adopted in this analysis using the bilinear stress-strain curve in figure 14.

Fiber-matrix failure by debonding is simulated by zeroing the tensile stiffness and stress of any fiber-matrix element where the bond strength is exceeded. This debonding causes the stresses in the remaining elements of that column to increase in order to support the tensile load. The displacements of the elements and column therefore increases. After debonding, the fiber-matrix element has unchanged compressive stiffness but zero tensile stiffness, i.e., it can sustain compressive but not tensile loads.

In the model, creep is estimated using relaxation data for the Ti-15-3 alloy. First a virtual creep stress is calculated for each column. The creep stress is virtual as it produces no change in the magnitude or sign of the real stress acting on the composite, but is used to estimate the magnitude of the driving force which produces the creep strain in the composite. The magnitude of the virtual creep stress in each column is obtained by averaging the virtual creep stress for each element in that column. The virtual creep stress in each element is obtained from the relaxation curve in figure 4 using the stress level of a given element and the time increment of interest. The creep displacement in each column is then obtained using the column stiffness and the virtual creep stress for that column. The creep strain of the composite is computed by summing the individual column displacements.

Tensile Analysis

Using the model described in the preceding section, the tensile stress-strain curve of the $[90]_8$ composite was analyzed. The bilinear stress-strain curve in figure 14 was used for the matrix, while the fiber was assumed to be elastic with a modulus of 345 GPa. The fiber distribution shown in figure 15 was used in this and subsequent analyses. Computationally this distribution was attained by first assigning a value of $L_f = 0.8$ to all fiber-matrix elements and then alternately adding and subtracting a random number between 0

5

and 0.1 to each fiber-matrix element over 50 iterations. As bond strength of the fiber-matrix interface is an unknown quantity, tensile analyses were run using three different bond strengths of 150, 350, and 550 MPa. The results of these analyses are presented in figure 16. Note that the best fit is obtained using a bond strength of 350 MPa. Further improvement in the fit was subsequently achieved by assuming a random distribution of bond strengths centered about 350 MPa. The improved fit (fig. 17) was obtained using a range of bond strengths between 150 and 550 MPa. The use of a range of bond strengths is probably physically more realistic than a single bond strength in a multifiber analysis.

While the fit achieved in figure 17 is excellent, the importance of this simple one-dimensional analysis is qualitative rather than quantitative in nature. The most important trends revealed by this tensile analysis are summarized here. First, the analysis confirms that the initial nonlinearity in the [90]$_8$ composite stress-strain curve of figure 17 is most likely resulting from fiber-matrix debonding. The average fiber-matrix bond strength is significantly lower than the flow stress of the Ti-15-3 alloy. Second, general matrix flow does occur, but only well after the onset of the debonding process. Finally, matrix creep in the short term tensile test was negligible.

While the effects of residual stresses are not directly included in this analysis, their impact on the accuracy of this analysis should be minor. The magnitude of any residual stresses at 426 °C should be small (ref. 6) when compared to that at room temperature. Further, the bond strength distribution determined in this analysis does partly account for the effect of residual stresses on fiber-matrix debonding.

Cyclic Deformation Analysis

The [90]$_8$ fatigue tests were analyzed with this model to help understand the observed deformation response. Modeling of fatigue tests was undertaken using the same assumptions and final parameters used in the tensile analysis. Analytical and experimental results of the strain-controlled fatigue tests on [90]$_8$ composite material will be compared and discussed in detail. Also, a brief comparison and discussion of the results for the load-controlled fatigue tests follows.

Experimental and analytical stress-strain loops for strain-controlled fatigue tests are reproduced in figure 18. As was the case for the tensile analysis, the inelastic strain on loading to 0.28 percent total strain in cycle one is, analytically, produced by fiber-matrix interface failure. It should be noted that not all fiber-matrix elements in the model have failed at this point. On unloading, the analytical and experimental composite stiffness is significantly less than the initial stiffness. Cycle two produces a linear analytical response and the composite stiffness is seen to retrace the unload line observed in cycle one. However, the experimental stress-strain behavior in cycle two is slightly nonlinear, displaying greater stiffness at lower strains. This could be due to the effects of closure at interface cracks which have irregular surface topography. This does not occur analytically as complex topographical aspects of failed interfaces are not considered in this one-dimensional model. The experimental and analytical mean stress decrease with continued cycling, as both the maximum and minimum stress levels drop as shown

6

in figure 19. Analytically, the decrease in mean stress results from matrix creep, as no further debonding occurs. Lack of debonding events after cycle one is a direct consequence of the stress-based, interface failure criteria used in the analysis. Near half-life, $N = 3000$, the predicted stress-strain response has stabilized and no further change occurs with continued cycling (fig. 18). Note the compressive stiffness is much greater than the tensile stiffness near half-life. This occurs analytically because debonded fiber-matrix elements can support load in compression but are unable to do so in tension. Experimentally, closure of debonded interfaces should contribute to stiffer composite response in compression. However, it would appear that the closure-induced increase in compressive stiffness is not as abrupt experimentally. This may, in part, explain the discrepancy in minimum stress levels between experiment and analysis. Between half-life and failure, a significant reduction in the maximum stress level is observed experimentally (fig. 18). This is probably caused by growth of large cracks extending into the matrix, and, hence, is not predicted by the model as interface debonding is the only type of cracking process included in the analysis.

In load-controlled fatigue tests, initial stress-strain response is very similar to strain-controlled response. However, the change in control mode now causes an increase in strain levels over the life of a test, as shown in figure 20. At this stress range, 103 MPa, the analytical and experimental stress-strain response is essentially linear, signifying negligible interface debonding initially. The analytical strain range remains constant but the mean strain increases with continued cycling. The analytical increase in mean strain is produced by matrix creep. However, the experimental response displays a measurable increase in strain range accompanying the increase in mean strain. The increase in experimental strain range is small at first but becomes quite pronounced after 1000 cycles and grows catastrophically after 9000 cycles. The initial increase in strain range is probably related to debonding and/or small cracks propagating into the matrix, however, the large change in strain range near the end of the test is almost certainly resulting from rapid growth of large cracks. Over a majority of the life it would appear that the increase in mean strain is predominantly related to matrix creep, as the predicted mean strain is in good agreement with the experimental value up to cycle 9000.

Fatigue Life Comparisons

While strain-controlled fatigue tests on the [90]$_8$ composite did yield longer lives than load-controlled tests, these lives were still far shorter than that of the Ti-15-3 alloy or the [0]$_8$ composite. Examination of the fracture surfaces suggested that fatigue cracks often initiated at fiber-matrix interfaces (fig. 21). This observation, coupled with the relatively low bond strengths of the fiber-matrix interfaces used in the analysis, suggest that the short fatigue life of the [90]$_8$ composite results largely from very weak fiber-matrix interface strength. Stress concentration effects associated with closely spaced fibers probably compound this problem. While creep has been shown to dramatically affect deformation response, its effect on fatigue life seems to be less pronounced. Changing to strain control, which severely limits creep, did not dramatically increase the life of the [90]$_8$ composite in relation to the Ti-15-3 alloy.

SUMMARY OF RESULTS

The 426 °C fatigue properties of a $[90]_8$ SiC/Ti-15-3 composite have been studied and show:

1. Initial deformation response became nonlinear near a tensile strain of 0.2 percent, producing a sizable decrease in composite stiffness thereafter.

2. Continued cycling produced significant changes in mean stress levels for strain-controlled tests, and mean strain levels for load-controlled tests.

3. Fatigue life was far shorter than that of the Ti-15-3 alloy in strain-controlled tests.

CONCLUSIONS

Many aspects of deformation response for the $[90]_8$ composite could be modeled successfully with a simple one-dimensional analysis, when fiber-matrix debonding and inelastic matrix behavior (creep and plasticity) were included. The need for a macroscopic crack(s) analysis is obviously required to more completely characterize deformation response in fatigue tests. Even so, this analysis suggests that the short life of the $[90]_8$ composite relative to the Ti-15-3 alloy is, in part, caused by weak fiber-matrix interfacial strength.

APPENDIX

The computer code used to predict $[90]_8$ composite behavior and a generalized flowchart for that code is listed below. The computer code was written in BASIC and was run on an IBM AT computer. The version shown here requires one to manually input stress and time increments, however, for analyzing fatigue tests, a control loop was added to automatically generate the desired number of stress or strain cycles.

DEFINE FIBER DISTRIBUTION
DEFINE BOND STRENGTH DISTRIBUTION
DEFINE FIBER/MATRIX PROPERTIES

INPUT STRESS & TIME INCREMENTS

CALCULATE TIME INDEPENDENT(ELASTIC/PLASTIC)
COLUMN DISPLACEMENTS

UPDATE ELEMENT STRESSES

RECALCULATE COLUMN DISPLACEMENT AND
ALL ELEMENT STRESSES WITHIN A COLUMN
IF THE BOND STRENGTH OF ANY ELEMENT
IN THAT COLUMN IS EXCEEDED

CALCULATE TIME DEPENDENT(CREEP)
COLUMN DISPLACEMENTS

SUM COLUMN DISPLACEMENTS TO OBTAIN
COMPOSITE STRAIN INCREMENT

UPDATE TOTAL STRESS & STRAIN

```
10 REM TRANSVERSE COMPOSITE ANALYSIS
20 REM WITH PLASTICITY CREEP AND INTERFACE FAILURE
30 INPUT "NR,NC";NR,NC
40 LF=0
50 DIM L(NR,NC),S(NR,NC),SO(NR,NC),B(NR,NC),Y(NR,NC),K(NC),D(NC),E(NR)
60 DIM SIA(10),BSS(NR,NC)
70 REM DEFINE COMPOSITE FIBER DISTRIBUTION (L MATRIX)
80 FOR R=1 TO NR
90 FOR C=1 TO NC
100 FOR I=1 TO NR STEP 2
110 IF R=I THEN L(R,C)=0!:GOTO 190
120 NEXT I
130 L(R,C)=.8
140 FOR I=1 TO 50
150 L(R,C)=L(R,C)+RND*RND
160 L(R,C)=L(R,C)-RND*RND*.7
170 IF L(R,C)>.99 OR L(R,C)<.01 THEN L(R,C)=.8
180 NEXT I
190 LF=LF+L(R,C)
200 PRINT USING " .###";L(R,C);
210 LPRINT USING " .###";L(R,C);
220 NEXT C
230 PRINT
240 LPRINT
250 NEXT R
260 PRINT "VF=";
270 LPRINT "VF=";
280 PRINT USING " .###";LF/(NR*NC)
290 LPRINT USING " .###";LF/(NR*NC)
300 REM INITIALIZE B,S,Y,D,K MATRICES
310 FOR C=1 TO NC
320 FOR R=1 TO NR
330 B(R,C)=1
340 S(R,C)=0!
350 SO(R,C)=0!
360 Y(R,C)=75!
370 IF L(R,C)=0! THEN B(R,C)=0
380 NEXT R
390 D(C)=0!
400 K(C)=0!
410 NEXT C
420 INPUT "BOND STRENGTH & SCATTER";BS,BSS
430 FOR C=1 TO NC
440 FOR R=1 TO NR
450 BSS(R,C)=BSS*(.5-RND)
460 PRINT R,C,BSS(R,C)
470 NEXT R
480 NEXT C
490 REM SET MATERIAL MODULI
500 EF=50000!
```

```
510 EM=11000!
520 PM=1000!
530 REM INITIALIZE STRESS AND STRAIN
540 LPRINT "EF,EM,PM,YS,BS"
550 LPRINT USING " #.##^^^^";EF,EM,PM,Y(1,1),BS
560 STRESS=0!:STRAIN=0!
570 REM INPUT STRESS AND TIME INCREMENT
580 INPUT "STRESS & TIME INC";SI,TIM
590 REM CALCULATE COMPOSITE STRESS AND STRAIN
600 REM ELEMENT DISP WITHIN A COLUMN ARE EQUAL
610 REM HOWEVER ELEMENT STRESSES WITHIN A COLUMN ARE NOT NECESSARILY EQUAL
620 REM TOTAL DISP=SUM OF THE COLUMN DISP
630 REM TOTAL COLUMN STRESS MUST EQUAL COMPOSITE STRESS
640 DISP=0!
650 FOR C=1 TO NC
660 K(C)=0!
670 FOR R=1 TO NR
680 REM CALCULATE ELEMENT STIFFNESS
690 IF ABS(S(R,C))>Y(R,C) THEN KM=PM ELSE KM=EM
700 IF L(R,C)=0! THEN E(R)=KM:GOTO 770
710 IF B(R,C)=1 THEN GOTO 740
720 IF CLOOP>4 THEN GOTO 740
730 GOTO 750
740 E(R)=1!/(L(R,C)/EF+(1!-L(R,C))/KM):GOTO 770
750 E(R)=0!
760 REM CALCULATE COLUMN STIFFNESS
770 K(C)=K(C)+E(R)
780 NEXT R
790 REM CALCULATE COLUMN DISP
800 DI=SI*NR/K(C)
810 D(C)=D(C)+DI
820 REM UPDATE ELEMENT STRESS & YIELD STRENGTH
830 SMAX=0!
840 FOR R=1 TO NR
850 S(R,C)=S(R,C)+DI*E(R)
860 IF S(R,C)>SMAX THEN SMAX=S(R,C)
870 IF ABS(S(R,C))>Y(R,C) THEN Y(R,C)=.9999*ABS(S(R,C))
880 NEXT R
890 PRINT "SMAX,DISP=";
900 PRINT USING " #.###^^^^";SMAX,D(C)
910 REM CALCULATE DISP
920 DISP=DISP+D(C)
930 NEXT C
940 STRESS=STRESS+SI
950 STRAIN=DISP/NC
960 PRINT "STRESS,STRAIN";
970 PRINT USING " #.###^^^^";STRESS,STRAIN
980 SOLD=STRAIN
990 REM CHECK FOR INTERFACE FAILURE COLUMN BY COLUMN
1000 FOR C=1 TO NC
```

```
1010 SI=0!
1020 REM CALCULATE STRESS CONCENTRATION FROM ANY BOND FAILURE
1030 FOR R=1 TO NR
1040 IF B(R,C)=1 AND S(R,C)>BS+BSS(R,C) THEN SI=SI+S(R,C)
1050 NEXT R
1060 REM GO TO NEXT COLUMN IF NO BOND FAILURES IN PRESENT COLUMN
1070 IF SI=0! THEN GOTO 1380
1080 K(C)=0!
1090 FOR R=1 TO NR
1100 REM CALCULATE ELEMENT STIFFNESS
1110 IF B(R,C)=1 AND S(R,C)>BS+BSS(R,C) THEN GOTO 1120 ELSE GOTO 1150
1120 B(R,C)=0
1130 S(R,C)=0!
1140 GOTO 1190
1150 IF ABS(S(R,C))>Y(R,C) THEN KM=PM ELSE KM=EM
1160 IF L(R,C)=0! THEN E(R)=KM:GOTO 1200
1170 IF B(R,C)=0 THEN GOTO 1190
1180 E(R)=1!/(L(R,C)/EF+(1!-L(R,C))/KM):GOTO 1200
1190 E(R)=0!
1200 NEXT R
1210 REM CALCULATE COLUMN STIFFNESS
1220 FOR R=1 TO NR
1230 K(C)=K(C)+E(R)
1240 NEXT R
1250 REM UPDATE DISPLACEMENTS
1260 DI=SI/K(C)
1270 D(C)=D(C)+DI
1280 DISP=DISP+DI
1290 REM UPDATE ELEMENT STRESS & YIELD STRENGTH
1300 FOR R=1 TO NR
1310 S(R,C)=S(R,C)+DI*E(R)
1320 PRINT "S(";R;C;")=";S(R,C)
1330 IF ABS(S(R,C))>Y(R,C) THEN Y(R,C)=.9999*ABS(S(R,C))
1340 NEXT R
1350 PRINT "STRESS, STRAIN";
1360 STRAIN=DISP/NC
1370 PRINT USING " #.###^^^^";STRESS,STRAIN
1380 NEXT C
1390 IF STRAIN=SOLD THEN GOTO 1420
1400 SOLD=STRAIN
1410 GOTO 990
1420 REM RELAX STRESSES
1430 FOR C=1 TO NC
1440 TDS=0!
1450 REM CALCULATE RELAXATION IN EACH ELEMENT AND FIND SUM FOR COLUMN
1460 FOR R=1 TO NR
1470 IF S(R,C)+SO(R,C)=0! THEN GOTO 1530
1480 ASTR=ABS(S(R,C)+SO(R,C))/2
1490 DS=.0052028+.0000418*ASTR+.0001788*ASTR^2
1500 DS=DS*((S(R,C)+SO(R,C))/(2*ASTR))*(TIM/60!)
```

```
1510 DS=DS*1!
1520 TDS=TDS+DS
1530 NEXT R
1540 REM CALCULATE COLUMN STIFFNESS USING ELASTIC CONSTANTS
1550 K(C)=0!
1560 FOR R=1 TO NR
1570 REM CALCULATE ELEMENT STIFFNESS
1580 IF L(R,C)=0! THEN E(R)=EM:GOTO 1620
1590 IF B(R,C)=0 AND S(R,C)=>0! THEN GOTO 1610
1600 E(R)=1!/(L(R,C)/EF+(1!-L(R,C))/EM):GOTO 1620
1610 E(R)=0!
1620 REM CALCULATE COLUMN STIFFNESS
1630 K(C)=K(C)+E(R)
1640 NEXT R
1650 REM CALCULATE COLUMN DISPLACEMENT DUE TO RELAXATION
1660 DI=TDS*NR/K(C)
1670 REM MODIFY DISPLACEMENTS BUT DO NOT MODIFY STRESSES
1680 D(C)=D(C)+DI
1690 DISP=DISP+DI
1700 PRINT "CREEP STRAIN";
1710 PRINT USING " #.###^^^^";DI/NC
1720 NEXT C
1730 STRAIN=DISP/NC
1740 PRINT "STRESS,STRAIN AFTER CREEP";
1750 PRINT USING " #.###^^^^";STRESS,STRAIN
1760 IF CYC=NLPT OR CYC=1 THEN GOTO 1770 ELSE GOTO 1790
1770 LPRINT "STRESS,STRAIN";
1780 LPRINT USING " #.###^^^^";STRESS,STRAIN
1790 FOR C=1 TO NC
1800 FOR R=1 TO NR
1810 SO(R,C)=S(R,C)
1820 NEXT R
1830 NEXT C
1840 GOTO 580
1850 END
```

REFERENCES

1. Moore, J.B.: Application of Advanced Materials for Turbomachinery and Rocket Propulsion. Application of Advanced Material for Turbomachinery and Rocket Propulsion. AGARD CP-449, AGARD, Nevilly-Sur-Seine, France, 1989, pp. 1.1-1.5.
2. Johnson, W.S.; Lubowinski, S.J.; and Highsmith, A.L.: Mechanical Characterization of Unnotched SCS-6/Ti-15-3 Metal Matrix Composites at Room Temperature. ASTM-STP-1080, 1990, pp. 193-218.
3. Gabb, T.P.; Gayda, J.; and MacKay, R.A.: Isothermal and Nonisothermal Fatigue Behavior of a Metal Matrix Composite. J. Compos. Mater., vol. 24, no. 6, June 1990, pp. 667-686.
4. El-Soudani, S.M.; and Gambone, M.L.: Strain-Controlled Fatigue Testing of SCS-6/Ti-6Al-4V Metal Matrix Composite. Fundamental Relationships Between Microstructures and Mechanical Properties of Metal Matrix Composites, P.K. Liaw and M.N. Gungor, eds., The Minerals, Metals and Materials Society, Warrendale, PA, 1990, pp. 669-704.
5. Lerch, B.A.; Gabb, T.P.; and MacKay, R.A.: Heat Treatment Study of the SiC/Ti-15-3 Composite System. NASA TP-2970, 1990.
6. Gayda, J.; Gabb, T.P.; and Freed, A.D.: The Isothermal Fatigue Behavior of a Unidirectional SiC/Ti Composite and the Titanium Alloy Matrix. Fundamental Relationships Between Microstructures and Mechanical Properties of Metal Matrix Composites, P.K. Liaw and M.N. Gungor, eds., The Minerals, Metals and Materials Society, Warrendale, PA, 1990, pp. 497-514.
7. Caruso, J.J.; Trowbridge, D.; and Chamis, C.C.: Finite Element Applications to Explore the Effects of Partial Bonding on Metal Matrix Composite Properties. NASA TM-101482, 1989.
8. Shimansky, R.A.; et al.: Effect of Interfacial Bonding on Transverse Properties of SiC/RBSN Composites. HITEMP Review 1989, NASA CP-10039, 1989, pp. 75.1-75.7.
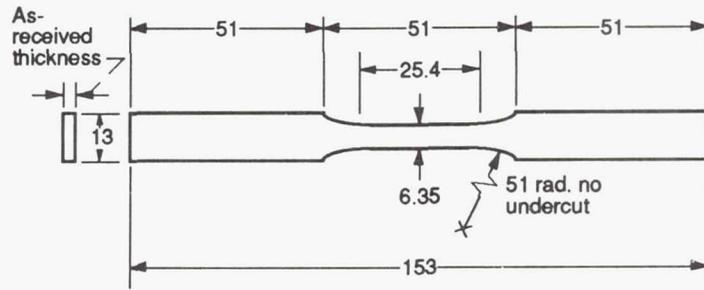
Figure 1.–SiC/Ti-15-3 composite test specimen. (All dimensions are in mm.)
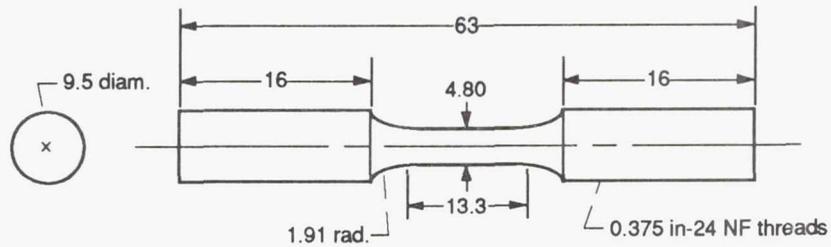
Figure 2.–Ti-15-3 alloy test specimen. (All dimensions are in mm.)
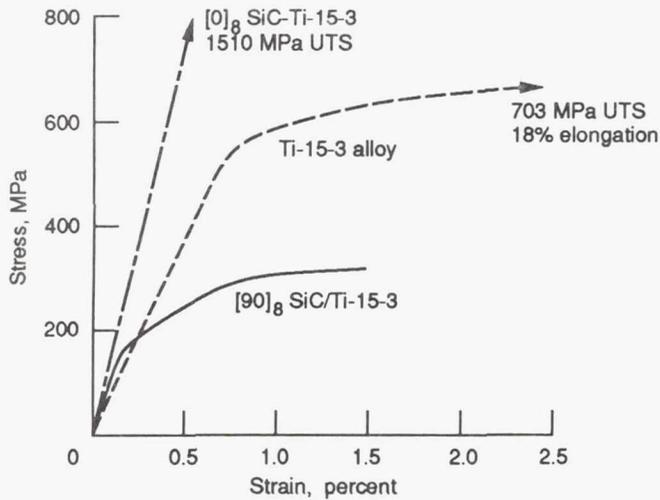
Figure 3.—Tensile curves of SiC/Ti-15-3 composite and the Ti-15-3 alloy.
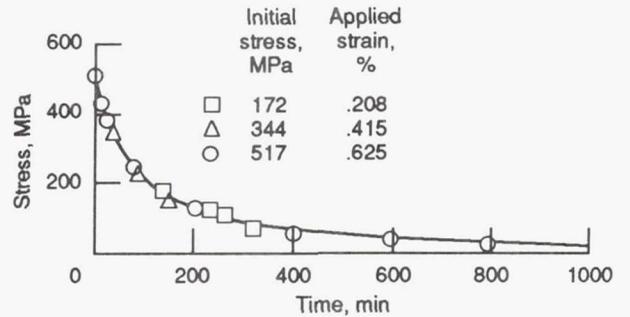
Figure 4.—426°C stress relaxation data for the Ti-15-3 alloy.

15
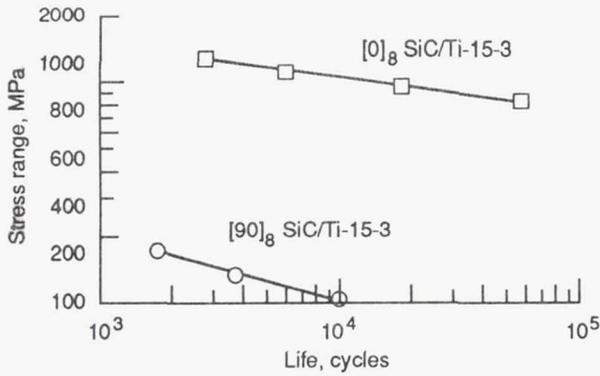
Figure 5.—Load-controlled fatigue life data for the [90]$_8$ and the [0]$_8$ composite.
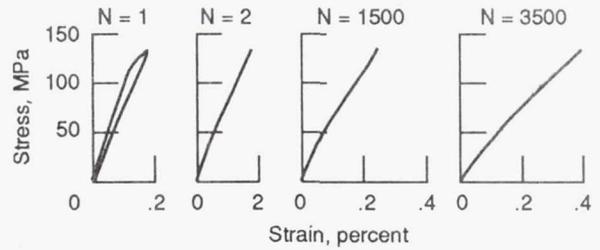

Figure 6.—Cyclic stress-strain response of the [90]$_8$ composite tested under load-control.
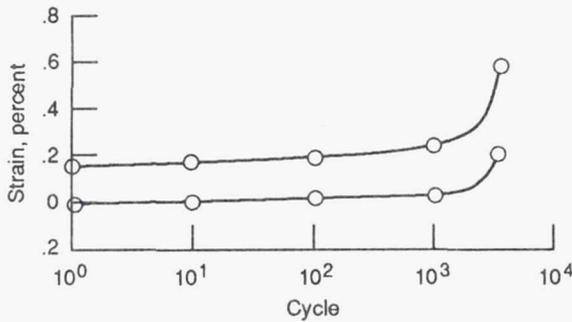

Figure 7.—Maximum and minimum strain levels of the [90]$_8$ composite at a stress range of 138 MPa.
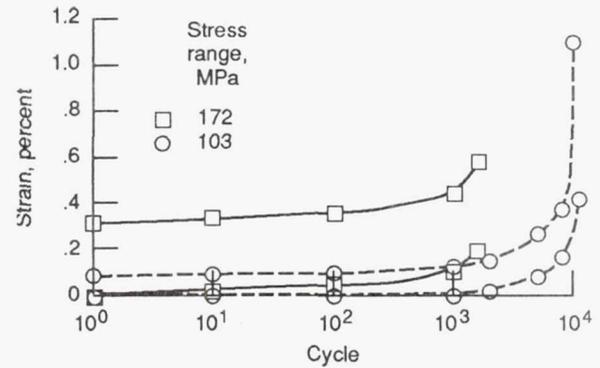
Figure 8.—Maximum and minimum strain levels of the [90]$_8$ composite at a stress range of 103 and 172 MPa.
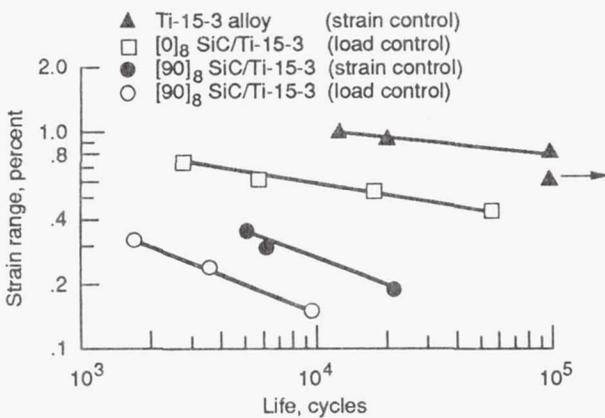
Figure 9.—Fatigue life versus strain range data for the composite and the Ti-15-3 alloy.
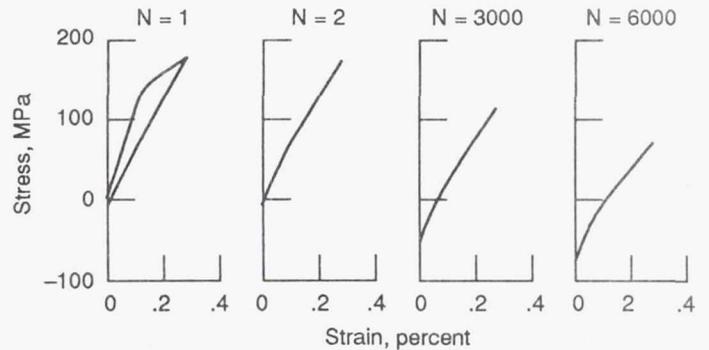
Figure 10.—Cyclic stress-strain response of the [90]$_8$ composite tested under strain-control.

16
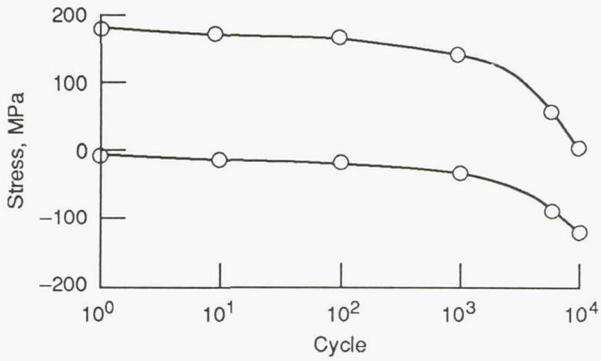
Figure 11.—Maximum and minimum stress levels of the $[90]_8$ composite at a strain range of 0.28%.
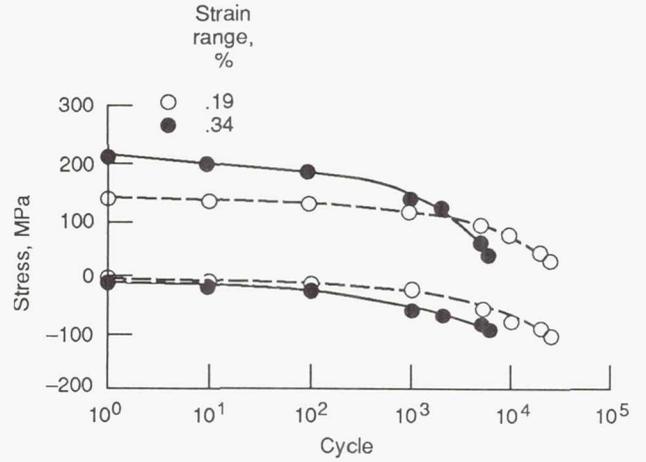

Figure 12.—Maximum and minimum stress levels of the $[90]_8$ composite at a strain range of 0.19 and 0.34%.
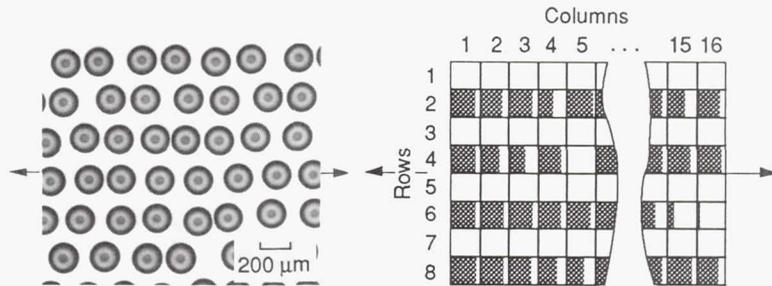
(a) Transverse specimen showing load orientation and fiber distribution.

(b) Simple one-dimensional composite model.
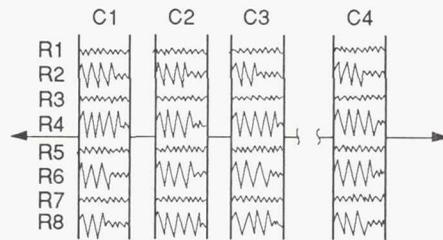
(c) Mechanical spring representation of the model showing how the elements of a given column are loaded in parallel to produce equivalent displacements while the columns are each subjected to the same transmitted load.

Figure 13.—Rationalization of composite model.

17
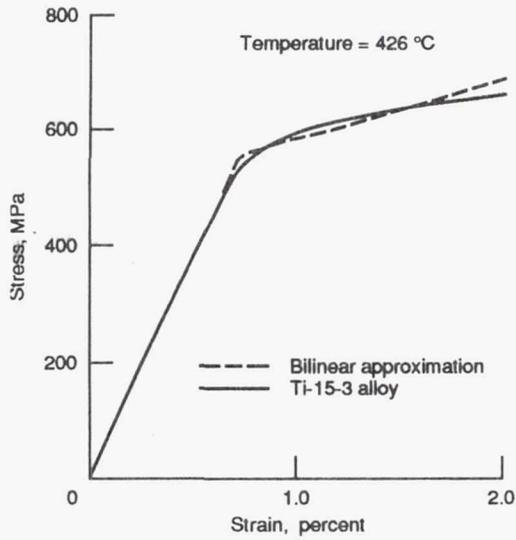
Figure 14.—Bilinear approximation of Ti-15-3 alloy tensile curve used to model composite response.

.000	.000	.000	.000	.000	.000	.000	.000	.000	.000	.000	.000	.000	.000	.000	.000
.800	.738	.800	.513	.885	.857	.531	.057	.800	.800	.928	.328	.663	.800	.597	.794
.000	.000	.000	.000	.000	.000	.000	.000	.000	.000	.000	.000	.000	.000	.000	.000
.842	.647	.444	.800	.106	.909	.606	.800	.652	.874	.794	.553	.800	.800	.800	.800
.000	.000	.000	.000	.000	.000	.000	.000	.000	.000	.000	.000	.000	.000	.000	.000
.800	.800	.800	.800	.800	.854	.434	.989	.800	.799	.800	.800	.800	.660	.212	.089
.000	.000	.000	.000	.000	.000	.000	.000	.000	.000	.000	.000	.000	.000	.000	.000
.868	.800	.741	.646	.573	.800	.933	.602	.774	.588	.793	.800	.711	.800	.800	.713

Figure 15.—Distribution of fiber spacing used in the analysis. Each number represents the fiber content of a given element.
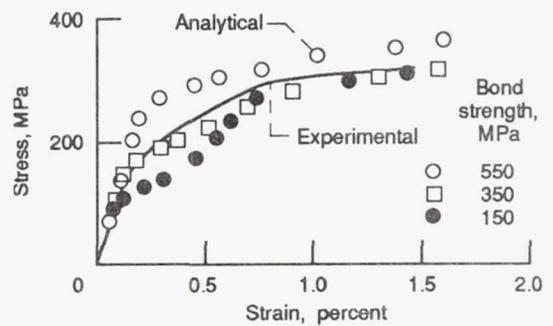

Figure 16.—Comparison of experimental and anlaytical tensile curves for the [90]$_8$ composite.

18

Figure 17.—Comparison of experimental and analytical tensile curves for the $[90]_8$ composite assuming a range of bond strengths.
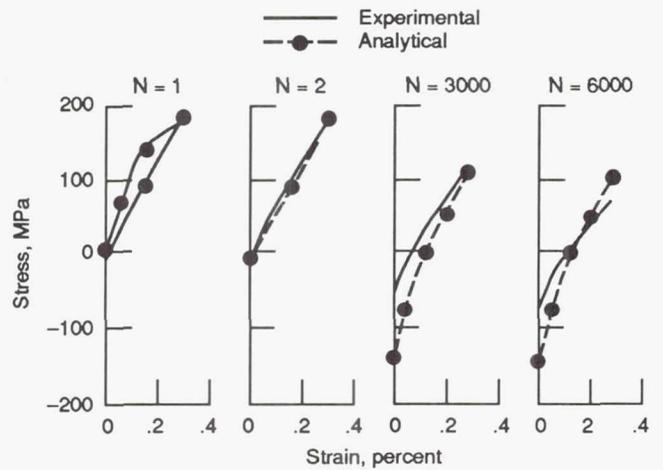

Figure 18.—Comparison of experimental and analytical stress-strain response for a strain-controlled fatigue test on $[90]_8$ composite.
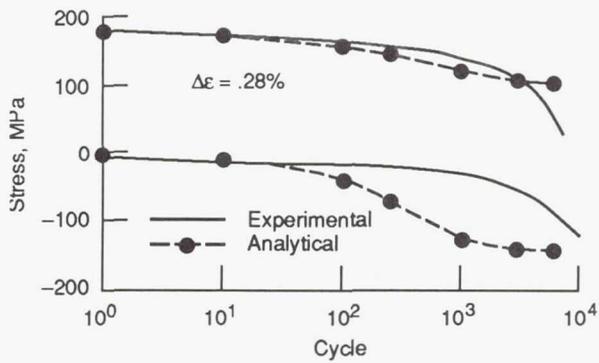

Figure 19.—Comparison of experimental and analytical stress levels for a strain-controlled fatigue test on $[90]_8$ composite.
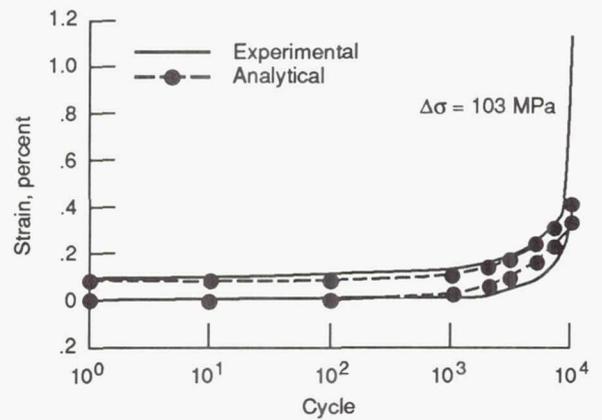

Figure 20.—Comparison of experimental and analytical strain levels for a load-controlled fatigue test on $[90]_8$ composite.
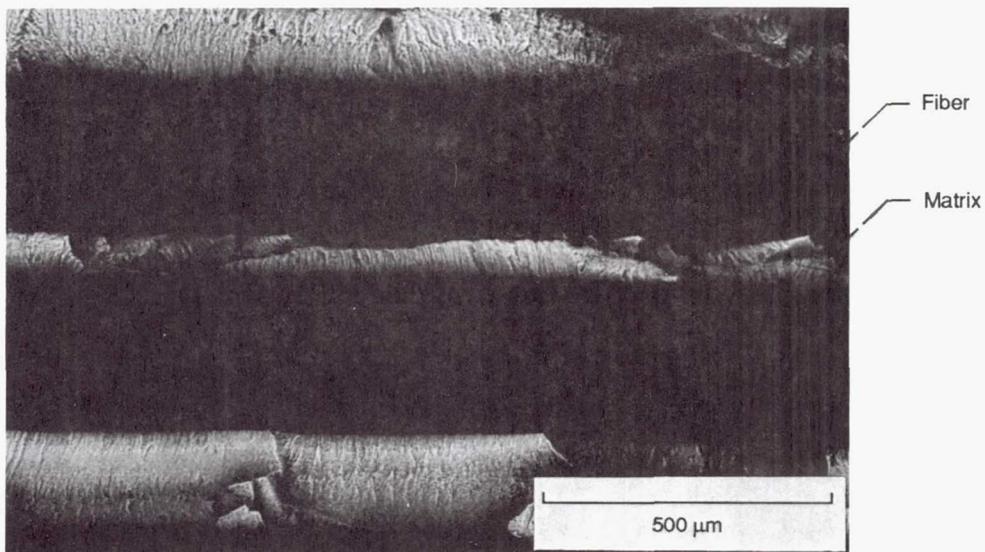

Figure 21.—Fracture surface of a $[90]_8$ composite fatigue specimen. Note initiation points at fiber matrix interfaces.

19

Report Documentation Page

1. Report No. NASA TM-103686	2. Government Accession No.	3. Recipient's Catalog No.

4. Title and Subtitle	5. Report Date
Isothermal Fatigue Behavior of a [90]8 SiC/Ti-15-3 Composite at 426 °C	January 1991
	6. Performing Organization Code

7. Author(s)	8. Performing Organization Report No.
John Gayda and Timothy P. Gabb	E-5904
	10. Work Unit No. 505-63-5A

9. Performing Organization Name and Address	11. Contract or Grant No.
National Aeronautics and Space Administration Lewis Research Center Cleveland, Ohio 44135-3191	
	13. Type of Report and Period Covered

12. Sponsoring Agency Name and Address	Technical Memorandum
National Aeronautics and Space Administration Washington, D.C. 20546-0001	14. Sponsoring Agency Code

15. Supplementary Notes

16. Abstract

The transverse fatigue behavior of a unidirectional, SiC/Ti-15-3 composite (35 v/o SiC, [90]8) was evaluated at 426 °C. The fatigue behavior of the composite along the fiber direction ([0]8) and of unreinforced Ti-15-3 alloy were also studied for comparison purposes. The [90]8 composite fatigue life was much shorter than [0]8 life. Further, [90]8 fatigue life was also found to be far lower than that of the unreinforced Ti-15-3 alloy. A simple, one-dimensional model for [90]8 fatigue behavior indicated that the short life of the composite in this orientation resulted, in large part, from weak fiber-matrix bond strength. This conclusion was supported by fractographic evidence showing numerous fatigue initiation sites along the fiber-matrix interfaces.

17. Key Words (Suggested by Author(s))	18. Distribution Statement
Fatigue SiC/Ti-15-3 composite	Unclassified – Unlimited Subject Category 24

19. Security Classif. (of this report) Unclassified	20. Security Classif. (of this page) Unclassified	21. No. of pages 20	22. Price* A03

NASA FORM 1626 OCT 86   *For sale by the National Technical Information Service, Springfield, Virginia 22161